Science of Sintering, **51** (2019) 339-351

doi:https://doi.org/10.2298/SOS1903339M

UDK: 622.782; 661.183.8

Electrochemical and Structural Properties of Ni(II)-alumina Composites as an Annealing Temperature Function

Zorica Mojović[1], Tatjana Novaković[1*)], Miloš Mojović[2], Tanja Barudžija[3], Miodrag Mitrić[3]

[1]University of Belgrade, Institute of Chemistry, Technology and Metallurgy, Department of Catalysis and Chemical Engineering, Njegoševa 12, 11000 Belgrade, Republic of Serbia

[2]Faculty of Physical Chemistry, University of Belgrade, Studentski trg 12-16, P.O.Box 47, 11158 Belgrade, Serbia

[3]Institute of Nuclear Sciences "Vinča", University of Belgrade, Mike Petrovića Alasa 12-14, Belgrade, Republic of Serbia

Abstract:

Alumina powders, pure and doped with nickel, were synthetized by sol-gel method and calcined at 500, 900 and 1100 ^oC in order to obtain mesoporous structures with a high specific surface area, well adapTab. to catalytic application. The characterization of samples was performed by XRD, EPR spectroscopy and electrochemical impedance spectroscopy (EIS). XRD analysis showed that the addition of Ni^{2+}, as well as the annealing temperature, affects the structural properties of the obtained composites. EPR analysis revealed the traces of Fe^{3+} impurities, the presence of oxy defects in alumina and Ni^{2+} in tetrahedral position for samples calcined at 1100 ^oC. The impedance of the Nafion/alumina modified GCE depended on combined effect of porous structure and surface properties of alumina samples. The electrochemical behavior of a glassy carbon electrode modified with Ni (II)-doped aluminas was studied in 0.5 M NaOH solution, with and without methanol. The electrochemical activity of nickel-doped alumina composites was dictated by the amount of present NiO impurity.

Keywords*: Alumina; Sol-gel; Nickel; Annealing temperature; Cyclic voltametry.*

1. Introduction

There is an increasingly growing interest in the electrochemistry of ordered solids based on zeolites, clays, layered double hydroxides with common a nanostructured porous inorganic matrix able to be permeated with organic and inorganic species [1]. Such materials comprise a variety of nanoarchitectures in relation to the shape and size of the crystals and their cavities, pores, channels, etc., from microporous to mesoporous, and a variety of guest's species. Adsorption capacity of these materials has motivated their exploitation in the electrochemistry domain for catalysis, energy production and storage, and sensing. Transition aluminas are important in the field of various catalytic processes because of their high specific surface areas, surface property and crystalline structure [2-7]. These properties of obtained alumina phases depend on the precursor, method of preparation, sample history and the calcinations conditions. The role of alumina in the catalyst system is often assumed to be

*) **Corresponding author:** tnovak@nanosys.ihtm.bg.ac.rs

purely physical acting as an inert solid onto which a catalyst can be dispersed. However, the surface of alumina is chemically reactive and is a catalyst for many acid/base reactions. Datka et al. showed that basic hydroxyl groups at alumina surface, that are absent at HY zeolite, can influence the reaction pathway [5].

It is known that properties of alumina can be modified by addition of different metals or metal oxides, as well as by changing the consolidation parameters [8, 9].

Nickel/alumina composites have found uses for various applications such as catalysts [2-4, 6, 7], coatings [10] or sensors [11], but low electrical conductivity of alumina-based ceramics is one of the reasons that prevent wider application in the field of electrocatalysis. Since alumina is considered as insulating material, nickel/alumina systems have not been investigated as electrode material, except from nickel particles deposited on conductive porous alumina [12] or as sensor for methanol vapor [11]. Electrochemical characterization can give additional insight in surface and structural properties of materials. Recently, electrochemical characterization of molecular species incorporated in non-conductive metal-organic frameworks was performed [13]. The electrochemical characterization of low loading catalyst, in non-conducting materials prepared in bulk can provide additional information for catalyst tailoring.

This paper presents the results of studies on the influence of calcination temperature on the structural and electrochemical properties of nickel-alumina composites with different Ni/Al ratio. The electrical properties and the activity of synthesized composites toward methanol electrooxidation were tested in order to investigate the activity of formed Ni-species. The aim of electrochemical investigation was to establish connection between electrochemical activity of investigated aluminas and data obtained by other characterization techniques.

2. Materials and Experimental Procedures

Ni(II)-doped alumina composites were prepared by sol-gel method using aluminum alkoxide as a precursor. To prepare boehmite sols, aluminum isopropoxide was hydrolyzed in an excess amount of water (100:1, H_2O:Al^{3+} mole ratio) at 80 ^oC, followed by peptization with the appropriate amount of HNO_3 (0.07:1, H^+: Al^{3+} mole ratio) to form a sTab. colloidal sol. The sol was kept at a constant temperature for the desired time under reflux conditions, during which most of the alcohol was evaporated [14]. The freshly prepared boehmite sol, pure and dopped with variable concentration of nickel nitrate solution, were mixed together and then vigorously stirred in order to obtain a homogeneous Ni(II)-doped boehmite sol. The molar ratios of Ni^{2+}/Al^{3+} were 0.1, 0.2 and 0.4, i.e. 10, 20 and 40 % of nickel. The pure and the doped boehmite sols were then gelled at 40 ^oC, during 24 hours, than at 100 ^oC in same time interval. The gels were heated from room temperature to the final temperature of 500, 900 and 1100 ^oC with the heating rate of 10 $^oCmin^{-1}$ and were kept for a 5 h. The samples obtained in this manner are designated as A-500, A-900 and A-1100 for pure alumina, where A stands for alumina and the number stands for final temperature. The samples containing Ni were designated as A10-500 and so on. The A stands for alumina, the first number describes the % of Ni in alumina sol, and the second number stands for final heating temperature.

The X-ray powder diffraction measurements were performed on a PHILIPS 1050 X-ray diffractometer using Ni-filtered Cu Kα radiation and Bragg-Brentano focusing geometry. The patterns were taken in the 5-90^o 2θ range with the step length of 0.05^o 2θ and exposure time of 5 s per step. The X-ray Line Profile Fitting Program (XFIT) with a Fundamental Parameters convolution approach to generating line profiles was used for the calculation of both the crystallite size and the microstrain parameter of the synthesized powders [15].

The electron paramagmetic resonance (EPR) spectra of the powder samples were recorded at room temperature by a Bruker Elexsys IIE540 spectrometer operating at *X*-band (9.5 GHz) with the following settings: modulation amplitude, 2 *G*; modulation frequency, 100 kHz; microwave power, 6.3 mW; scan range, 514 mT; scan time, 4 min. The spectra were recorded and analyzed using the Xepr software (Bruker BioSpin Germany).

In order to use the investigated alumina powders as electrode materials, the samples were homogeneously dispersed in original 5 wt.% Nafion® solution using an ultrasonic bath. Droplets (10 μl) of these suspensions (containing 1 mg of alumina powder) were placed on the surface of a glassy carbon electrode (area = 0.0314 cm^2). After solvent evaporation, the alumina was uniformly distributed on the glassy carbon support in the form of a layer. For the electrochemical investigations in a three-electrode glass cell, the alumina-modified glassy carbon electrode (GCE) was used as working electrode. The reference electrode was Ag/AgCl in 3M KCl, while a platinum foil served as a counter electrode. The electrochemical measurements were performed using Autolab electrochemical workstation (Autolab PGSTAT302N, Metrohm-Autolab BV, Netherlands). Cyclic voltammetry was performed at scan rate of 50 mVs^{-1} from 0.5M NaOH with and without 0.5M methanol. Impedance measurements were carried out at constant potential using a 5 mV rms sinusoidal modulation in the 10 kHz-10 mHz frequency range from 0.5 M NaOH.

3. Results and Discussion

3.1. X-ray diffraction

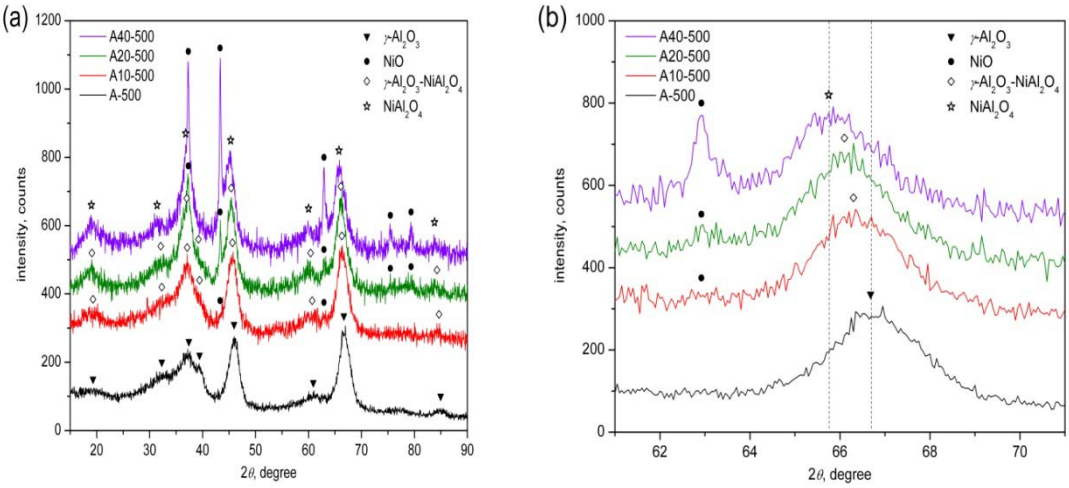

Fig. 1. XRD patterns of pure and Ni-doped alumina samples calcined at 500 ^oC and their phase compositions at (a) 15-90° and (b) 61-71° 2theta range.

X-ray diffraction patterns of alumina samples annealed at 500 ^oC (A-500, A10-500, A20-500 and A40-500) are presented in Fig. 1a. As can be seen, A-500 sample contains reflections characteristic of a cubic *γ*-alumina (*γ*-$Al_{2.144}O_{3.2}$, PDF No. 79-1558), which has spinel-type lattice that contains cation vacancies [16]. This was expected, since the boehmite transforms to *γ*-alumina at about 450 ^oC [17]. The XRD pattern of A10-500 sample still has all the characteristic reflections of *γ*-alumina, but the intensities of some reflections change and their positions slightly move to the left (Fig. 1b), since the *d*-spacing increase. This indicates that Ni (or more precisely, NiO) is incorporated into the spinel structure and *γ*-alumina-$NiAl_2O_4$ solid solution is formed due to nonstoichiometric composition [18, 19]. A small impurity of NiO (PDF No. 89-3080) is also detecTab.. With further increase of Ni

content in alumina samples A20-500 and A40-500, positions of diffraction reflections keep moving to the left, which means that a greater amount of nickel is incorporated into the spinel structure and for sample A40-500 a spinel $NiAl_2O_4$ phase (PDF No. 73-0239) is stabilized. Also with increasing Ni-doped level, amount of NiO impurity increases. Formation of NiO alongside nickel aluminate is common phenomenon [20].

Microstructural parameters of all samples were obtained using the model of isotropic broadening of diffraction peaks due to isotropic shape of crystallites and isotropic microstrain (Tab. I). Crystallite size and microstrain of γ-alumina phase in A-500 sample are 6.1 nm and 0.8 %, respectively. A considerably high value of microstrain (imperfection of crystal structure) arises from the presence of a large number of cation vacancies and that is why the γ-alumina, is known as a defect spinel [21]. According to Tsybulya et al. [22], vacancies in low-temperature Al_2O_3 polymorphs (such as γ-alumina) are not statistically distributed point defects but ordered chains associated with the planar faulting. Such stacking faults are the main origin of the broadening of diffraction peaks. Hence, the values of microstrain parameters of our samples, obtained using the isotropic model, should be taken as a first approximation. Microstrain in A10-500 sample of spinel phase corresponding to a solid solution of γ-alumina-$NiAl_2O_4$ was somewhat higher than for pure alumina sample, amounting 0.9 %. This result indicated that the small amount of Ni introduce some more defects in already defect spinel structure. A decrease of microstrain values with further increase of Ni content (Tab. I) indicates that more stabilized spinel structure appears, due to less cation vacancies.

Tab. I Calculated values of the crystallite size and microstrain parameters.

Sample	Crystallite size (nm)		Microstrain (%)	
	alumina/$NiAl_2O_4$/ $Ni_2Al_{18}O_{29}$	NiO	alumina/$NiAl_2O_4$/ $Ni_2Al_{18}O_{29}$	NiO
A-500	6.1		0.8	
A10-500	4.1		0.9	
A20-500	4.6		0.64	
A40-500	3.3	16.6	0.42	0.018
A-900	8		0.7	
A10-900	8.2		0.6	
A20-900	12.7		0.59	
A40-900	12.9	22.7	0.47	0.131
A-1100	135		0.22	
A10-1100	18.3		0.3	
A20-1100	30.1		0.89	
A40-1100	14.7	36.5	0.002	0.001

Fig. 2a shows the results of X-ray diffraction analysis of alumina samples annealed at 900 ^oC (A-900, A10-900, A20-900 and A40-900). The XRD pattern of pure alumina sample (A-900) could be assigned to a mixture of tetragonal δ-alumina (δ-Al_2O_3, PDF No. 16-0394) [16] and monoclinic θ-alumina (θ-$Al_{2.427}O_{3.64}$, PDF No. 79-1559). δ-alumina can be formed from γ-alumina during the calcination at 700-800 ^oC [23], while θ-alumina could be formed from δ-alumina during the calcinations at 900-950 ^oC [23]. However, it can be seen that Ni-doped alumina samples calcined at 900 ^oC crystallized neither in tetragonal δ-alumina structure, nor in monoclinic θ-alumina structure. These samples crystallized in cubic spinel

structure, indicating that nickel stabilizes the cubic spinel structure. Positions of diffraction reflections obtained fo samples calcined at 900 °C move to the left (Fig. 2b) with an increase of Ni content, same as for Ni-doped alumina samples calcined at 500 °C. This shift indicated that a greater amount of nickel is incorporated into the spinel structure. In samples A10-900 and A20-900 γ-alumina $NiAl_2O_4$ solid solution is formed due to the nonstoichiometric compositions, while in sample A40-900 a main phase is a spinel $NiAl_2O_4$. A10-900 sample has all the characteristic reflections of the spinel structure, without visible reflections of NiO impurity. Reflections of NiO impurity start to appear in the XRD pattern of A20-900 sample and then increase in the XRD pattern of A40-900 sample.

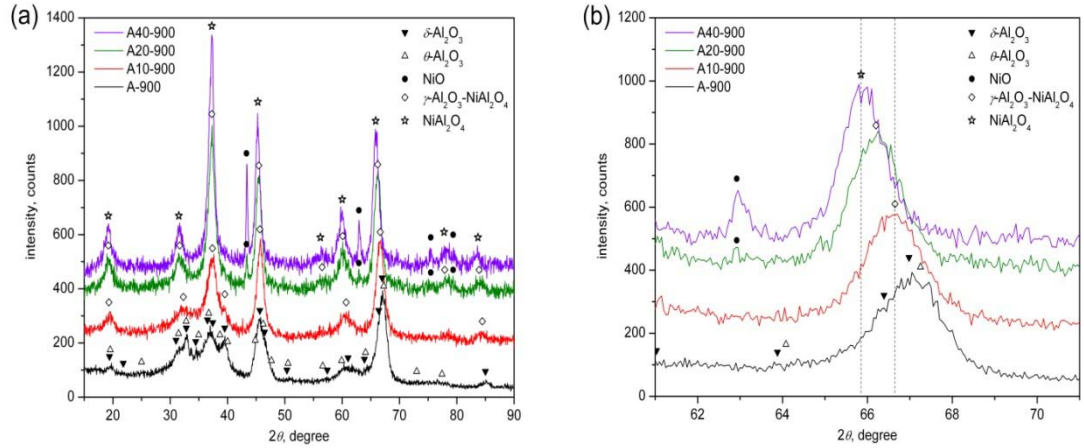

Fig. 2. XRD patterns of pure and Ni-doped alumina samples calcined at 900 °C and their phase compositions at (a) 15-90° and (b) 61-71° 2theta range.

Phase composition of alumina samples annealed at 1100 °C (A-1100, A10-1100, A20-1100 and A40-1100) is shown in Fig. 3. The XRD pattern of A-1100 sample contains only reflections characteristic of a rhombohedral α-alumina (α-Al_2O_3, PDF No. 81-2266). In samples A10-1100 and A20-1100 the main phase is monoclinic $NiAl_{10}O_{16}$ ($5Al_2O_3 \cdot NiO$, PDF No. 37-1292), which is a metasTab. B phase [24]. In these samples α-alumina remains, but as minor phase. In sample A20-1100 both, monoclinic $NiAl_{10}O_{16}$ and spinel $NiAl_2O_4$ phases are present, whereby, the spinel $NiAl_2O_4$ is in the formation process. With further increase of Ni content in sample A40-1100 monoclinic phase $NiAl_{10}O_{16}$ vanishes and dominant phase becomes spinel $NiAl_2O_4$, with some amount of NiO impurity.

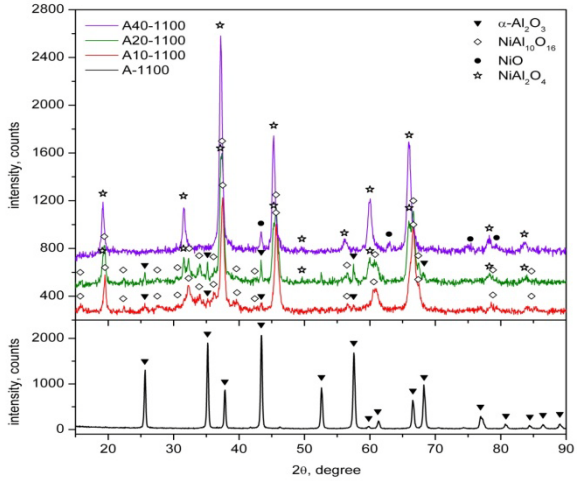

Fig. 3. XRD patterns of pure and Ni-doped alumina samples calcined at 1100 °C and their phase compositions.

3.2. Electron paramagnetic resonance (EPR) spectroscopy

Electron paramagnetic resonance (EPR) spectroscopy provides information about the existence of unpaired electrons. The g-factor from calculated characteristic resonance line of EPR spectra can be used to analyze paramagnetic center's electronic structure. The EPR spectra of all investigated samples are presented at Fig. 4. The EPR spectra of non-doped alumina samples recorded at 77 K (Fig. 4) showed two main peaks at g = 4.23 and g = 2.00.

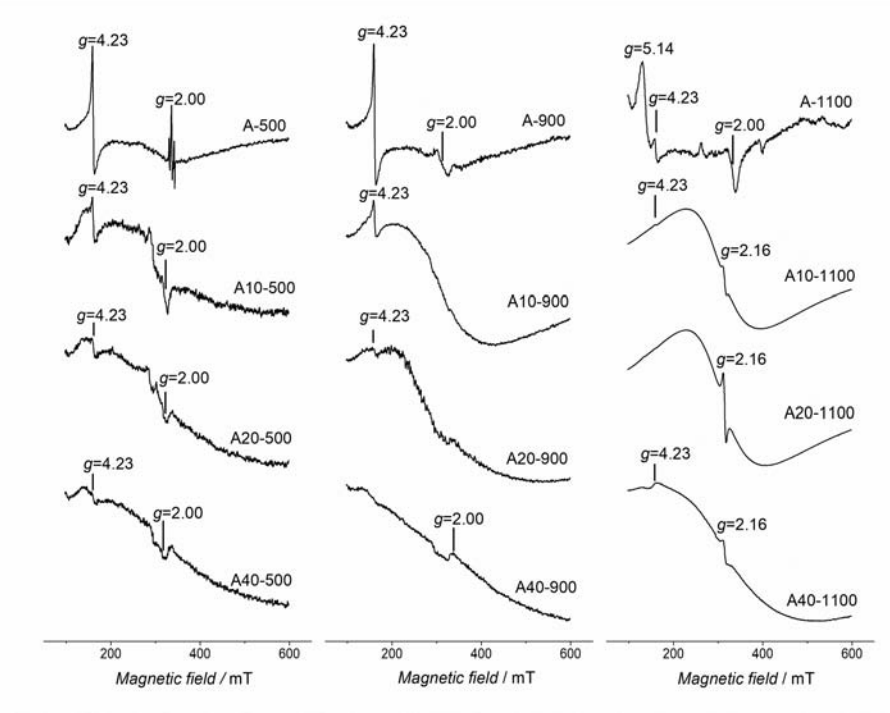

Fig. 4. EPR spectra of pure and Ni(II)-doped-alumina samples recorded at 77 K.

Literature data show that the low field EPR signal with g = 4.23 can be ascribed to isolated Fe^{3+} ions in regular or distorted octahedral and tetrahedral positions [25]. Iron and silicon are the key trace impurities in aluminum isopropoxide used as precursor for alumina synthesis [26]. This signal decreased with the increase of Ni^{+2} content in Ni-doped alumina indicating that the surrounding of Fe^{3+} ion was changed. Similar decrease of signal intensity was noticed in glass matrix with the increase of iron content [27, 28]. The decrease was ascribed to the decrease of amount of isolated iron ions due to the increased density of paramagnetic ions. The signal intensity decrease in our experiment can be explained in similar fashion. The addition of nickel disrupted isolated positions of Fe^{3+} ions leading to the decrease of signal.

The signal of A-500 at g = 2.00 showed hyperfine structure. Paramagnetic site in the alumina that can give rise to hyperfine structure are located on aluminum center Al [29] or on aluminum-oxygen hole center [30]. The nuclear spin of ^{27}Al is 5/2 causing the signal originating from these paramagnetic sites to split. The hyperfine structure could not be observed for the EPR spectra of non-doped alumina calcined at 900 and 1100 ^{o}C. This can be ascribed to the formation of different paramagnetic site than above mentioned. It is considered that oxy defect has Al-O-O$^{\bullet}$ structure in which the distance between aluminum atom and the electron spin is long enough to neglect the hyperfine interaction with Al [31]. The EPR spectra of Ni-doped aluminas calcined at 500 and 900 ^{o}C showed that introduction of nickel in alumina structure led to decrease of g = 2.00 signal intensity. Similar decrease was noticed for

Tb^{3+} doped sol-gel derived alumina films [31] and ascribed to the bond formation between Tb^{3+} and oxy defect.

The EPR spectra obtained for Ni-doped alumina calcined at 1100 ^{o}C were significantly different. Low field EPR signal was shifted to g = 5.14 for sample A-1100 indicating the change of the surrounding of the iron ion. The literature data ascribe this line to the Fe^{3+} ion in α-alumina [32]. Additionaly, these spectra were dominated by broad wave at low magnetic field. The sharp peak at g = 2.16 was observed for all Ni-doped sample calcined at 1100 ^{o}C. This g value is attributed to Ni^{2+} ions in octahedral coordination [33]. $NiAl_2O_4$ spinel or NiO phases containing octahedral coordinated Ni^{2+} ions are found on the surfaces of nickel/alumina catalysts [34]. The highest intensity for this g value was observed for A20-1100 sample. According to XRD analysis, the signal at g = 2.16 probably originated from nickel in $NiAl_{10}O_{16}$, since this form of Ni-aluminate was observed only with samples calcined at 1100 ^{o}C.

3.3. Electrochemical impedance spectroscopy

The characterization of the Nafion/alumina modified GCE was performed by the electrochemical impedance spectroscopy. For a modified electrode, the Nyquist plot (Fig. 5) shows characteristic semi-circle pattern due to barrier to the interfacial electron-transfer.

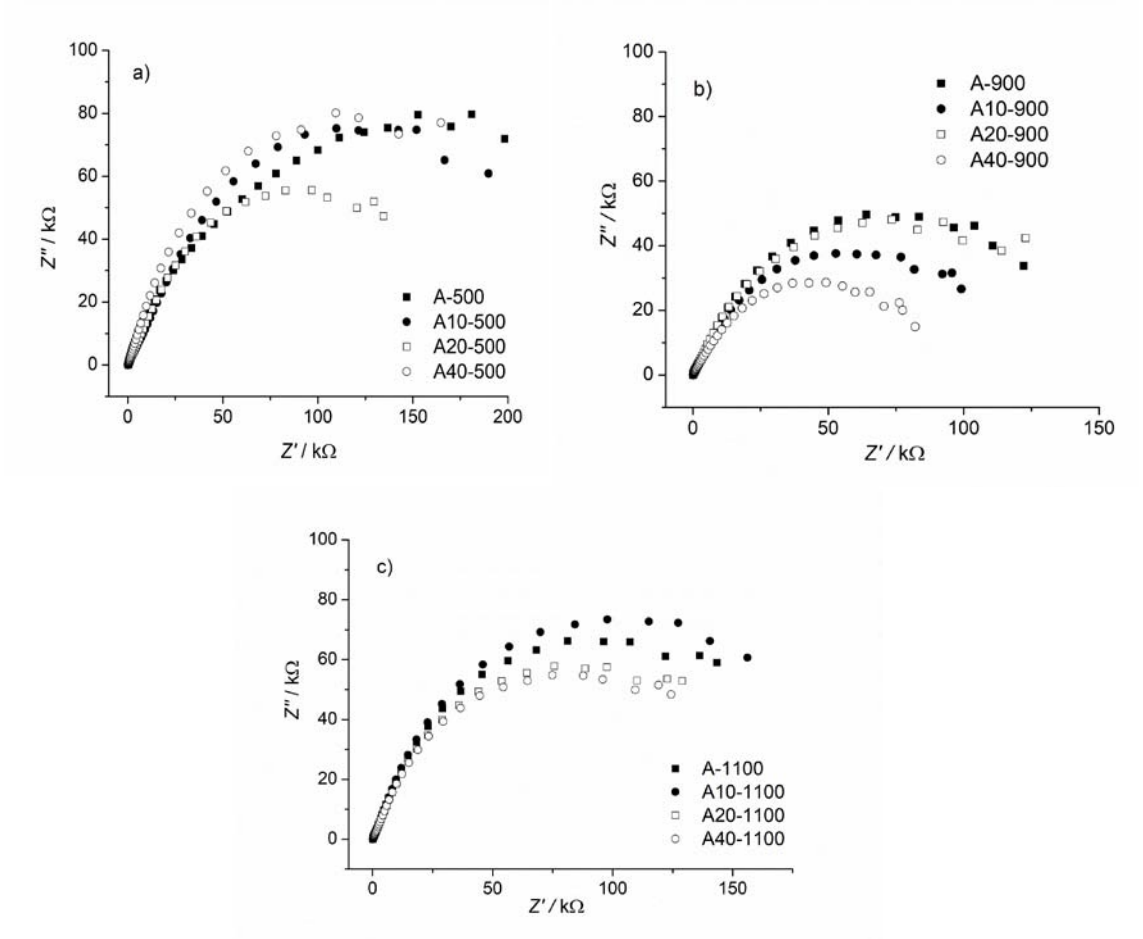

Fig. 5. Nyquist plot for alumina and nickel-doped alumina calcined at a)500 ^{o}C, b)900 ^{o}C and c)1100 ^{o}C recorded at OCP in 0.5 M NaOH.

The Nyquist plot of all Nafion/alumina samples almost overlapped at high frequencies, while more obvious variation of traces occurred at lower frequencies. The impedance data (Fig. 5) were fitted to simplified Randles circuit (Fig. 6), that consists of internal resistance (R_S) in series with the parallel combination of charge transfer resistance R_{ct} and constant phase element CPE (designated as Q) instead of true capacitor.

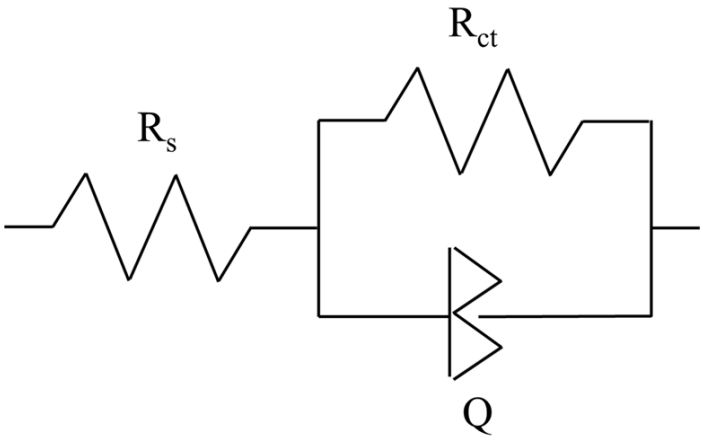

Fig. 6. The equivalent electric circuit used to fit EIS data.

CPE usually represents the double layer capacitance and can be described by following equation:

$$Z = \frac{1}{Y_0(jw)^n}$$

where Y_0 is CPE admittance, j is the imaginary unit, w is the angular frequency and n is CPE exponent which is associated with the system inhomogeneity. The capacitance element CPE will be pure capacitance when $n = 1$ while it will be pure resistance when $n = 0$. For values $0.5 < n < 1$ and CPE is non-ideal capacitor that is influenced by surface heterogeneity.

In this circuit model R_s represents the solution resistance and it amounted around 50 Ω for all investigated samples. The values of circuit elements obtained by fitting were presented in Tab. II.

Tab. II The electrochemical parameters extracted from the EIS data recorded in 0.5 M NaOH.

Sample	R_{ct} (kΩ)	Y (μS s^n)	n
A-500	256	1.74	0.70
A10-500	227	2.91	0.71
A20-500	184	4.13	0.70
A40-500	217	4.02	0.70
A-900	166	5.05	0.72
A10-900	131	5.20	0.70
A20-900	161	5.00	0.72
A40-900	100	5.38	0.69
A-1100	179	3.60	0.80
A10-1100	195	3.49	0.80
A20-1100	155	3.72	0.80
A40-1100	149	3.76	0.80
GCE+Nafion	118	3.97	0.83

The EIS measurements were performed at OCP (about 0.18 V vs. Ag/AgCl), where was no electron transfer process, leading to large values of resistance [35, 36].

The variation of parameters was determined by surface and textural properties of alumina samples imbedded in Nafion, i.e. by porous structure of Nafion/alumina samples and penetration of electrolyte in pores. According to Song et. al. [37] impedance of porous electrode is determined by penetrability and pore size distribution. Increase of impedance is obtained for increased penetrability and smaller pore size distribution and vice versa. According to results obtained from nitrogen adsorption-desorption isotherms (presented elsewhere [38] specific surface area and pore volume decreased with increase of calcination temperature and nickel content. The reduced porosity led to increased penetrability and decreased impedance as obtained for sample annealed at 900 ^{o}C. However, samples annealed at 1100 ^{o}C showed largest pore sized distribution that probably was cause of increase of impedance.

When alumina is immersed in aqueous solution, double layer is formed as the result of electrostatic interaction between ions in solution and the surface charge of the alumina [39]. The surface charge is mostly created of $-AlO^-$ and $-AlOH^{2+}$ groups [40]. The surface charge profile is influenced by dehydration and the change of phases with the annealing temperature [39, 41]. The variation of admittance of constant phase element was most pronounced for series of samples calcined at 500 ^{o}C. The introduction of nickel in alumina samples calcined at 500 ^{o}C influenced surface charge distribution more than in samples calcined at higher temperatures. XRD and EPR analysis showed that sample A-500 had more defects than samples calcined at higher temperatures. Both analysis showed that introduction of nickel stabilized the structure.

3.4. Cyclic voltammetry

The nickel species formed during in synthesized samples were characterized by cyclic voltammetry. In order to test electrochemical activity of introduced nickel GCE modified with synthesized material was tested in alkaline solution. The electrodes were cycled up to ten times in order to test stability of Ni-doped aluminas. The stability of alumina samples increased with increase of nickel content and with increase of calcination temperature. The 10th successive cycle for each investigated sample are presented in Fig. 7a and b. Cyclic voltammograms recorded in 0.1M NaOH for A10-500 only showed current rise at high anodic potential due to oxygen evolution reaction. With increase of Ni content in sample characteristic Ni(II) $\rightarrow$ Ni(III) pair of peaks appeared at potential range 0.3-0.6 V vs. Ag/AgCl electrode and was well pronounced for A40-500 sample. The redox Ni(II) $\rightarrow$ Ni(III) originates from electroactive layer of $Ni(OH)_2$ that is formed over Ni-containing species upon immersion in alkaline solution. The current of oxygen evolution also increased with increase of Ni content, as expected since Ni-based electrodes are good catalyst for the OER [42]. The current of NiOOH formation decreased with the increase of calcinations temperature of samples (Fig. 7b). The XRD analysis showed that NiO was formed in samples annealed at 500 ^{o}C. A40-900 contained NiO, while A40-1100 contained mixture of Ni-oxide forms. The electrochemical activity of Ni-modified alumina samples was probably also influenced by alumina surface charge.

Further testing was performed in the reaction of methanol oxidation from alkaline solution. The continuous cyclic voltammetry in methanol containing alkaline solution was performed and the 30th cycles for each electrode are presented in Fig. 8. The current rise due to methanol oxidation was observed at same potential as the formation of NiOOH. There was no current of NiOOH reduction during reverse scan. The same dependence of current of methanol oxidation on Ni content and calcinations temperature as for the current of NiOOH formation was observed. The characteristic feature of recorded voltammograms is hysteresis

between the anodic and the cathodic sweeps, in which a higher methanol oxidation charge is observed in the cathodic sweep. Broadening of cathodic limit to hydrogen evolution resulted in higher current of methanol oxidation in forward than in reverse scan (not shown). This can be ascribed to reactivation of the electrode by the reduction of surface oxides in the region of hydrogen evolution [43, 44].

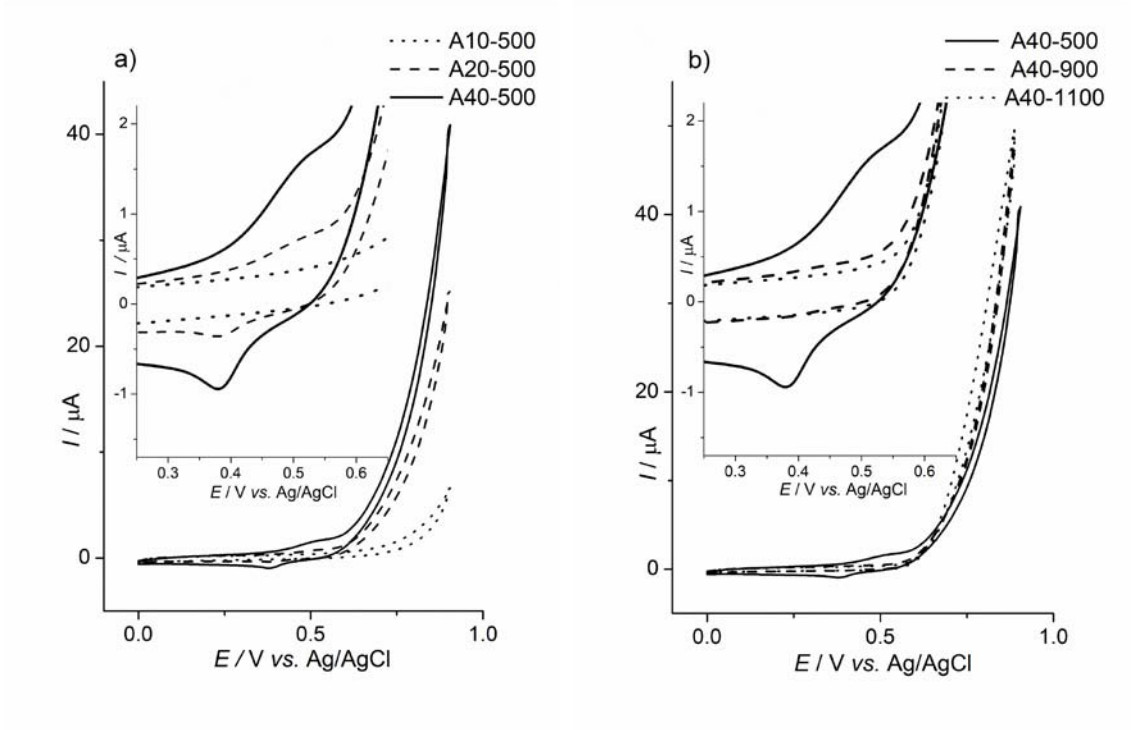

Fig. 7. Cyclic voltammograms of alumina samples in 0.5M NaOH: a) samples at same temperature with increased Ni content; b) samples with same Ni content at different temperatures. Inset: enlarged part of CV in potential range 0.25-0.6 V.

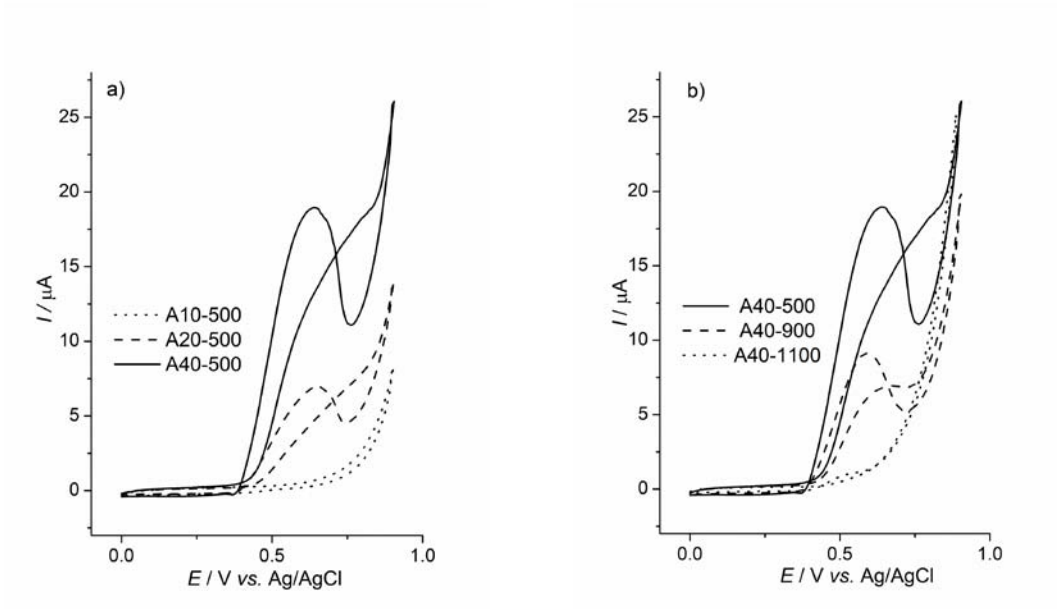

Fig. 8. Cyclic voltammograms of alumina samples in 0.5M CH_3OH + 0.5M NaOH: a) samples at same temperature with increased Ni content; b) samples with same Ni content at different temperatures.

The electrochemical activity of nickel-doped alumina samples was dictated by the amount of formed $Ni(OH)_2$, i.e. methanol electrooxidation current was correlated with the amount of present NiO. The sample A10-500, where all nickel was dissolved in γ-alumina, showed only oxygen evolution current. The low methanol electrooxidation current (around 1 μA) obtained for A40-1100 sample could be expected. XRD analysis showed that most of nickel was incorporated in $NiAl_2O_4$ spinel while NiO was present in very small amount.

It is unclear how much Ni inside alumina structure affects the electrochemical response of nickel-doped alumina. According to Ojani et al. [45], who investigated Ni-modified zeolite Y, the presence of Ni ions inside zeolite cages beside Ni ions present on the surface of the zeolite was essential for good electrochemical activity of NiY. It was proposed that the methanol oxidation takes place on the oxy-hydroxide species formed on the surface of the electrode, while nickel species incorporated in zeolite act as an electron relay to the $Ni(OH)_2$/NiOOH redox system. It can be speculate that this kind of synergy effect was observed for samples annealed at 500 ^oC. The samples annealed at higher temperatures have sTab. Ni-spinel structure as main phase and synergy effect was probably absent.

4. Conclusion

Alumina samples dopped with different amount of nickel were synthetized by sol-gel method and annealed at 500, 900 and 1100 ^oC.

XRD diffraction analysis has confirmed that the phase composition of Ni-doped alumina samples, as well as crystallite size and microstrain of detected phases, were dependent on the amount of Ni added and the annealing temperature. With increase of Ni content dominant phase becomes spinel $NiAl_2O_4$, with some amount of NiO impurity, which indicates that nickel stabilizes the spinel structure. Formation of NiO alongside nickel aluminate is common phenomenon.

The EPR spectra revealed the presence of Fe^{3+} impurities in alumina samples originating from starting chemical for synthesis. This signal decreased with the increase of Ni^{+2} content in alumina indicating that introduction of Ni ions changed the surrounding of Fe^{3+} ions. The EPR spectra obtained for Ni-doped alumina annealed at 1100 ^oC showed the sharp peak at g = 2.16 attributed to Ni^{2+} ions in $NiAl_{10}O_{16}$.

EIS study confirmed that the impedance of the Nafion/alumina modified GCE depended on combined effect of porous structure and surface properties of alumina samples. The electrochemical activity of nickel-doped alumina composites was dictated by the amount of present NiO impurity. The activity of NiO in the samples toward methanol oxidation greatly depended on the cathodic limit indicating that the methanol oxidation was mainly governed by the nature of the electrode surface.

The amount and structure of nickel content in catalyst are of great importance. The results presented in this paper can be used as guidelines for tailoring of Ni-alumina composites synthesis for future applications.

Acknowledgments

This work was supported by the Ministry of Education, Science and Technological Development of the Republic of Serbia, (Project Nos. III 45001, ON 172015, III 41005).

5. References

1. A. Doménech-Carbó, A .Walcarius, J. Solid State Electrchem., 19 (7) (2015) 1885.
2. Y. Li, J. Su, R .Li, Micropor. Mesopor. Mat., 243 (2017) 9.
3. F . Bentaleb, E. Marceau, Micropor. Mesopor. Mat., 156 (2012) 40.
4. Q. He, T. Gan, D. Zheng, Sh. Sh. Hu, J. Solid State Electrochem., 14 (6) (2010) 1057.
5. J. Datka, Z.Sarbak, R. P. Eischens, J. Catal., 145 (1994) 544.
6. C. H. Bartholomew, J. Catal., 45 (1976) 41.
7. J. Zieliński, J. Catal., 76 (1982) 157.
8. P. Milanović, M.M. Vuksanović, M. Mitrić, D. Stojanović, A. Kojović, J. Rogan, R. Jančić-Hainemann, Sci. Sinter., 50 (2018) 77.
9. S. Filipović, N. Obradović, S. Marković, A. Đorđević, I. Balać, A. Dapčević, J. Rogan, V. B. Pavlović, Sci. Sinter., 50 (2018) 409.
10. W. Buchner, R. Schliebs, G. Winter, KH. Buchel Industrial inorganic chemistry. Wiley, Weinheim, Germany 1989.
11. J. Vijaya, J, J. L. Kennedy, G. Sekaran, B. Jeyaraj, KS. Nagaraja, J. Hazard Mater., 153 (2008) 767.
12. C. Hai, J. Liu, H. Watanabe, M. Fuji, F. Wang, M. Takahashi, J. Am. Cer. Soc., 92 (2009) S38.
13. E. Mijangos, S. Roy, S. Pullen, R. Lomoth, S. Ott, Dalton Trans., 46 (2017) 4907.
14. B. E. Yoldas, Am. Ceram. Soc. Bull., 54 (1975) 289.
15. R.W.Cheary, A. Coelho, J. Appl. Crystallogr., 25 (1992) 109.
16. R.-S. Zhou, R. L. Snyder, Acta Crystallogr B., 47 (1991) 617.
17. BC. Lippens, JH. De Boer, Acta Crystallogr., 17 (1964) 1312.
18. E. Kiš, R. Marinković-Nedučin, G. Lomić, G. Bošković, D. Ž. Obradović, J.Kiurski, P. Putanov, Polyhedron, 17 (1998) 27.
19. AAS. Gonçalves, MJF. Costa, L. Zhang, F. Ciesielczyk, M. Jaroniec, Chem. Mater., 30 (2) (2018) 436.
20. MM. Guraya, SP. Catán, MD. Sánchez, S. Moreno, SSRG Int. J. Appl. Chem., 3 (2016) 1.
21. G. Gutierrez, A. Taga, B. Johansson, Phys. Rev. B., 65 (2001) 012101.
22. SV. Tsybulya, GN. Kryukova Phys. Rev. B., 77 (2008) 024112.
23. H. De Souza Santos, PK. Kiyohara, P. De Souza Santos, Mater. Res. Bull., 31 (1996) 799.
24. P. Bassoul, JC. Gilles, J. Solid State Chem., 58 (1985) 383.
25. L. Bonneviot, M. Che, K. Dyrek, R. Schollner, G. Wendt, J. Phys. Chem., 90 (1986) 2379.
26. K-E. Khishigbayar, W-S. Tak, Y-G. Moon, K. B. Shim, C. J. Kim, J. Ceram. Process Res.,15 (6) (2014) 514.
27. I .Ardelean, M. Peteanu, D. S. Filip, V. Simon, G.Györffy, Solid State Commun., 102 (1997) 341.
28. S.T. dos Reis, W. M. Pontuschka, J. B. Yang, D. L. A. Faria, Materials Research., 6 (2003) 389.
29. R. Schnadt, A. Räuber, Solid State Commun., 9 (1971) 159.
30. H. Hosono, Y. Abe, J. Non-Cryst. Solids., 95–96 (1987) 717.
31. T. Ishizaka, S. Tero-Kubota, Y. Kurokawa, T. Ikoma, J. Phys. Chem. Solids., 64 (2003) 801.
32. R. Stösser, G. Scholz, J-Y. Buzaré, G. Silly, M. Nofz, D. Schultze, J. Am. Ceram. Soc., 88 (2005) 2913.

33. H. B. Premkumar, D. V. Sunitha, H. Nagabhushana, S. C. Sharma, B. M. Nagabhushana, C. Shivakumara, J. L. Rao, R. P. S. Chakradhar, J. Lumin., 135 (2013) 105.
34. V. B. Kazansky, I. V. Elev, B. N. Shellmov, J. Mol. Catal., 21(1983) 265.
35. O. M. S. Filipe, C. M. A. Brett, Electroanalysis, 16 (2004) 994.
36. C. Gouveia-Caridade, C. M. A. Brett, Electroanalysis, 17(2005) 549.
37. H-K. Song, Y-H. Jung, K-H. Lee, L.H. Dao, Electrochim. Acta, 44 (1999) 3513.
38. A. Ivanović-Šašić, T. Novaković, Z. Mojović, Ž. Čupić, D. Jovanović, Sci. Sinter., 50 (3) (2018) 313.
39. B. Kasprzyk-Hordern, Adv. Colloid Interface Sci., 110 (2004) 19.
40. R. Sprycha, J. Colloid Interf. Sci., 127 (1) (1989) 1.
41. E. G. Kovaleva, L. S. Molochnikov, D. P. Stepanova, A. V. Pestov, D. G. Trofimov, I. A. Kirilyuk, A. I. Smirnov, Cell. BioChem. Biophys., 75 (2) (2017) 159.
42. N. Spinner, W. E. Mustain, Electrochim. Acta, 56 (2011) 5656.
43. M. A. Abdel Rahim, R. M. Abdel Hameed, M. W. Khalil, J. Power Sources., 134 (2004) 160.
44. C.-C. Hu, T.-C. Wen, Electrochim. Acta, 43 (12-13) (1998) 1747.
45. R. Ojani, J.-B. Raoof, S. Fathi, S. Alami-Valikchali, J. Solid State Electrchem., 15 (2011) 1935.

Садржај: *Прахови алумине, без додатка и са додатком никла, синтетисани су сол-гел методом и жарени на 500, 900 и 1100 °C с циљем да се добију мезопорозне структуре са високом специфичном површином, применљиве у каталитичке сврхе. Карактеризација узорака вршена је са XRD, EPR и EIS спектроскопијом. XRD анализа показала је да и додатак Ni^{2+}-јона, као и температура жарења, утичу на структурне особине добијених композита. EPR анализом утврђено је присуство Fe^{3+}-јона у траговима, окси-дефеката у алумини и Ni^{2+}-јона у тетраедарским позицијама у узорцима жареним на 1100 °C. Импеданса стакло-карбон електроде модификоване нафион/алумином, зависила је од комбинованог ефекта порозне структуре и површинских карактеристика узорака алумине. Електрохемијско понашање модификоване стакло-карбон електроде испитивано је у 0.5M раствору NaOH, без и са метанолом. Електрохемијска активност никл-алумина композита диктирана је присуством NiO фазе.*

Кључне речи*: Алумина, Сол-гел, Никл, Температура жарења, Циклична волтаметрија.*